atoms

MDPI

Article

Cross Sections and Rate Coefficients for Rovibrational Excitation of HeH^+ Isotopologues by Electron Impact

Mehdi Ayouz [1,*,†] and Viatcheslav Kokoouline [2,†]

1 LGPM, CentraleSupélec, Université Paris-Saclay, 8-10 rue Joliot-Curie, 91 190 Gif-sur-Yvette, France
2 Department of Physics, University of Central Florida, Orlando, FL 32816, USA
* Correspondence: mehdi.ayouz@centralesupelec.fr; Tel.: +33-175-316-603
† These authors contributed equally to this work.

Received: 29 May 2019 ; Accepted: 28 June 2019 ; Published: 5 July 2019

Abstract: Cross sections and thermal rate coefficients for rotational and vibration excitation of the four stable isotopologues of the $^4HeH^+$ ion by electron impact are presented. The data are calculated using a previously developed theoretical approach. The obtained rate coefficients are fitted to analytical formulas with the 10–10,000 K interval of applicability. These present results could be useful in tokamak plasma and astrophysical modeling and can help in the detection of these species in the interstellar medium.

Keywords: helium hydride ion; isotopologues; rovibrational excitation; R-matrix; quantum-defect theory; interstellar medium

1. Introduction

Over the past decades, it was suggested that the hydrohelium (helium hydride) cation HeH^+ can be present and observed in a number of astronomical environments, and particularly, in the planetary nebulae NGC 7027 [1–3]. In the interstellar medium (ISM), it is the process of radiative association of He and H^+ or of He^+ and H that forms the ion [4,5]. However, only very recently, the presence of the ion was confirmed by Güsten et al. [6] with the observation of the rotational ground-state transition of HeH^+ in the planetary nebula NGC 7027. These observations were made possible due to advances in terahertz spectroscopy [7] and high-altitude observatories [8]. Previously, a transition with a wavelength very similar to that of the $j = 1 \rightarrow 0$ rotational transition was found by Liu et al. [9]. However, further analysis suggested that it was actually caused by the CH molecule [10].

HeH^+ is easily formed in helium–hydrogen plasma, and in particular, in the hydrogen fusion reaction. The ion, with its isotopologues, plays an important role in the chemistry taking place in tokamaks, especially in the divertor region of the devices. Rovibrationally excited states, formed in collisions of HeH^+ with electrons, can be used for plasma diagnostics. The other process involving the HeH^+ isotopologues and electrons and taking place in the divertor and near walls of the reactors is the process of dissociative recombination. The process removes the ions from the plasma creating neutral atoms, which contribute to the damage of reactor walls.

There have been several experimental and theoretical studies [11–16] reporting cross sections for the dissociative recombination. Cross sections for vibrational excitation and de-excitation of the three lowest vibrational states of the ion by electron impact were also calculated previously [17]. However, the presence of vibrational resonances in the collisional spectra was ignored in that study. Čuríк and Greene [18] have recently reported cross sections for rotational excitation of HeH^+ collisions, where the Rydberg series of rovibrational resonances were accounted for.

Data relevant to the other isotopologues $^4HeD^+$, $^3HeH^+$, and $^3HeD^+$ could also be useful for plasma modeling and diagnostics in fusion reactors. In this respect, cross sections as well as rate

coefficients for collisions of the HeH^+ isotopologues with electrons are needed. To our knowledge, there is no such theoretical or experimental data available for the HeH^+ isotopologues.

In a previous study [19] (hereafter referred to as paper I), we reported cross sections and rate coefficients for vibrational excitation for transitions between the five lowest vibrational levels. In a further study [20] (hereafter referred to as paper II), we presented similar data for rotational transitions in collisions of $^4HeH^+$ with electrons. In the present study, as a follow-up of papers I and II, we determine cross sections and rate coefficients for vibrational and rotational (de-)excitation for collisions of the four stable HeH^+ isotopologues with electrons.

The rest of the article is organized in the following way. The next section briefly discusses the theoretical approach used in the present calculation. A detailed description of the approach is presented at length in papers I and II, so we restrict ourselves here only to underline its major ideas. In Sections 3 and 4, the obtained rate coefficients for vibrational and rotational (de-)excitation are discussed and compared with the data available in the literature. Section 5 concludes the study.

2. Theoretical Approach

Similarly to papers I and II, the present theoretical method uses the UK R-matrix code [21,22] with the Quantemol-N interface [23] and some elements of the quantum defect theory (MQDT) [24–26]. The same parameters (the basis and orbital spaces, the R-matrix size, etc.) as in Paper II were employed in the electron-scattering calculations. As a first step in the theoretical approach, the body-frame scattering matrix $\hat{S}^{\Lambda}(R)$ is obtained numerically for a number of internuclear distances R from $R = 0.85$ to $R = 3.95$ with a step of 0.05 bohr. At the second step, vibrational wave functions $\psi_v(R)$ for the four isotopologues are computed by solving the Schrödinger equation for vibrational motion using a DVR-type method [27].

Energies for vibrational and rotational transitions for the four isotopologues are shown in Tables 1 and 2 and compared with available data [28,29]. Note that unlike the present study, where the `aug-cc-pVQZ` basis is employed, in paper I, we used the `cc-pVQZ` basis to compute the potential energy curve (see Figure 2 of paper I). As a result, the obtained vibrational energies for the $^4HeH^+$ ion are slightly different in the present study and paper I.

Table 1. Energies $\Delta_v = E_{v+1} - E_v$ for vibrational transitions $v \to v + 1$ and rotational constants B_v of the $^4HeH^+$ and $^4HeD^+$ molecules used in this study and compared with data available in the literature. All values are in cm^{-1}.

Level v	$^4HeH^+$				$^4HeD^+$		
	Δ_v	Δ_v [29]	B_v	B_v [28]	Δ_v	B_v	B_v [28]
0	2910.8	2911.0007	33.523	33.558	2309.9	20.326	20.349
1	2604.4	2604.1676	30.808	30.839	2125.7	19.061	19.084
2	2296.2	2295.5787	28.074	28.090	1941.5	17.795	17.814
3	1983.0	1982.0562	25.282	25.301	1755.9	16.515	16.532
4	1661.6	1660.3559	22.389	22.402	1567.8	15.212	15.226
5	1329.5	1327.7860	19.338	19.344	1376.1	13.872	13.884
6	986.6	984.3599	16.061	16.058	1179.7	12.480	12.490
7	641.6	639.1959	12.492	12.479	977.9	11.019	11.025
8	328.0	327.3615	8.638	8.621	771.2	9.469	9.471
9	115.2	116.1487	4.854		562.8	7.810	7.808
10	25.6	24.4099	2.064		362.4	6.041	6.036
11					192.0	4.216	4.217
12					79.6	2.541	2.557

Table 2. Energies $\Delta_v = E_{v+1} - E_v$ for vibrational transitions $v \to v+1$ and rotational constants B_v of the ^{3}HeH$^+$ and ^{3}HeD$^+$ molecules used in this study. All values are in cm^{-1}.

Level v	^{3}HeH$^+$		^{3}HeD$^+$	
	Δ_v	B_v	Δ_v	B_v
0	2994.7	35.681	2422.7	22.514
1	2668.1	32.693	2218.4	21.036
2	2339.4	29.682	2013.8	19.555
3	2004.7	26.602	1807.5	18.056
4	1660.7	23.400	1598.0	16.525
5	1304.5	20.008	1383.8	14.944
6	937.4	16.345	1163.9	13.295
7	573.2	12.340	937.6	11.551
8	261.0	8.054	706.8	9.687
9	77.4	4.107	478.2	7.684
10	15.9	1.496	270.8	5.567
11	16.8	0.733	118.8	3.495
12	24.3	0.940	38.6	1.836

Scattering Matrix for Rovibrational Excitations in the HeH$^+$ Molecule and Its Isotopologues

The next step in the treatment is the vibrational and rotational frame transformations. If we neglect the rotational structure of the ion, which corresponds to an experiment where cross sections for vibrational transitions $v \to v'$ are averaged over all possible initial and summed over allowed final rotational states of the levels v and v', the theoretical cross section is obtained from the following scattering matrix:

$$\mathcal{S}^{\Lambda}_{\lambda' v' l', \lambda v l} = \left\langle \psi_{v'}(R) \left| S^{\Lambda}_{\lambda' l', \lambda l}(R) \right| \psi_v(R) \right\rangle , \tag{1}$$

where the brackets imply an integration over the vibrational coordinates. As a second step, the rotational frame transformation is accomplished using the matrix elements $\mathcal{S}^{\Lambda}_{\lambda' v' l', \lambda v l}$ of Equation (1), leading to the laboratory-frame scattering matrix

$$\mathcal{S}^{J}_{j' \mu' l' v', j \mu l v} = \sum_{\lambda \lambda'} (-1)^{l' + \lambda' + l + \lambda} C^{j' \mu'}_{l' - \lambda' J \Lambda'} C^{j \mu}_{l - \lambda J \Lambda} S^{\Lambda}_{l' \lambda' v', l \lambda v} , \tag{2}$$

where J is the total angular momentum of the e^--HeH$^+$ system, j, μ and j', μ' are the angular momenta with their projections on the molecular axis of the target before and after the rotational excitation of HeH$^+$ (and its isotopologues), and $C^{j' \mu'}_{l' - \lambda' J \Lambda'}$ and $C^{j \mu}_{l - \lambda J \Lambda}$ are Clebsch–Gordan coefficients. A detailed derivation of Equation (2) is given in Appendix A of paper II.

The matrices of Equations (1) and (2) are energy-independent and do not describe vibrational and rovibrational Rydberg resonances present in the collisional spectra. The actual scattering matrices $\mathcal{S}^{phys}$ are obtained from those two matrices, applying the closed-channel elimination procedure [24,26] as discussed in paper I. The total energy E of the system is the sum $E = E_{el} + E_{j \mu v}$ of the relative kinetic energy E_{el} of a collision and the energy $E_{j \mu v}$ of the initial state of the target.

3. Rate Coefficients and Cross Sections for Vibrational (De-)Excitation

The cross section for purely the vibrational transition $v \to v'$ is [30]

$$\sigma_{v' \leftarrow v}(E_{el}) = \frac{\pi \hbar^2}{2 m_e E_{el}} \sum_{\lambda' l' \lambda l} \left| \mathcal{S}^{phys}_{\lambda' l' v', \lambda l v} - \delta_{\lambda l v, \lambda' l' v'} \right|^2 , \tag{3}$$

where m_e is the reduced mass of the electron-ion system. Figure 1 demonstrates, as examples, the cross sections of Equation (3) for the $v = 3 \to v' = 0, 1, 2, 4$ transitions of ^{4}HeH$^+$ (solid lines) and ^{4}HeD$^+$ (dashed lines). At very low scattering energies, below 0.001 eV, the de-excitation cross sections behave

as $1/E_{el}$ according to the Wigner threshold law [31]. At higher energies, all the (de-)excitation cross sections vary significantly due to the presence of series of Rydberg resonances.

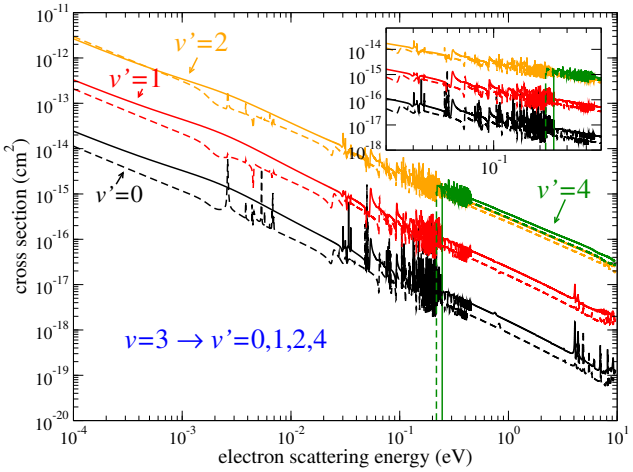

Figure 1. Cross sections of vibrational (de-)excitation from the vibrational level $v = 3$ to several other levels v' of ^{4}HeH$^+$ (solid lines) and ^{4}HeD$^+$ (dashed lines).

Figures 2 and 3 show thermally averaged rate coefficients (see Equation (13) of paper I) computed for transitions between the lowest vibrational levels for the four ^{4}HeH$^+$ isotopologues. The uncertainty of the rate coefficients for all transitions is about 5–30% for different temperatures. Due to the general E_{el}^{-1} dependence of the cross sections, the calculated rate coefficients $\alpha_{v'\leftarrow v}$ behave as $1/\sqrt{T}$ as functions of temperature T for de-excitation and as $\exp\left(-\Delta_{v'\,v}/T\right)/\sqrt{T}$ for excitation transitions, where $\Delta_{v'\,v} = E_{v'} - E_v$ is the excitation energy. Therefore, similarly to papers I and II, for convenience of use, the rate coefficients are fitted to the formula

$$\alpha^{fit}_{v'\leftarrow v}(T) = \frac{1}{\sqrt{T}} e^{-\frac{\Delta_{v'v}}{T}} P^{fit}_{v'v}(x)\,, \tag{4}$$

where $P^{fit}_{v'v}(x) \approx P^{fit}_{vv'}(x)$ are functions weakly dependent on temperature interpolated by a cubic polynomial

$$P^{fit}_{v'v}(x) = a_0 + a_1 x + a_2 x^2 + a_3 x^3 \qquad \text{and} \qquad x = \ln(T)\,, \tag{5}$$

with

$$\Delta_{v'v} = \begin{cases} E_{v'} - E_v > 0 & \text{for excitation}\,, \\ 0 & \text{for (de-)excitation}\,. \end{cases} \tag{6}$$

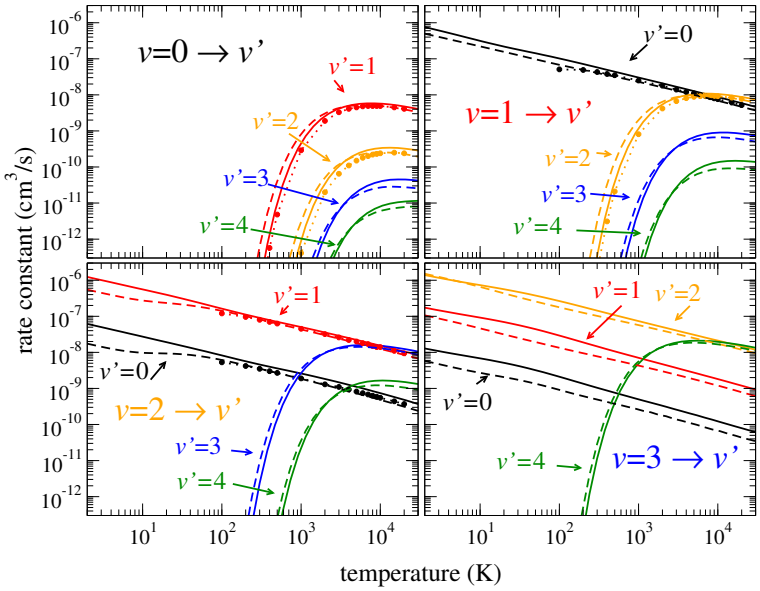

Figure 2. Examples of thermal rate coefficients for vibrational transitions in $^4HeH^+$ (solid lines) and $^4HeD^+$ (dashed lines). Results of a previous calculation [17] are shown by dotted lines with circles.

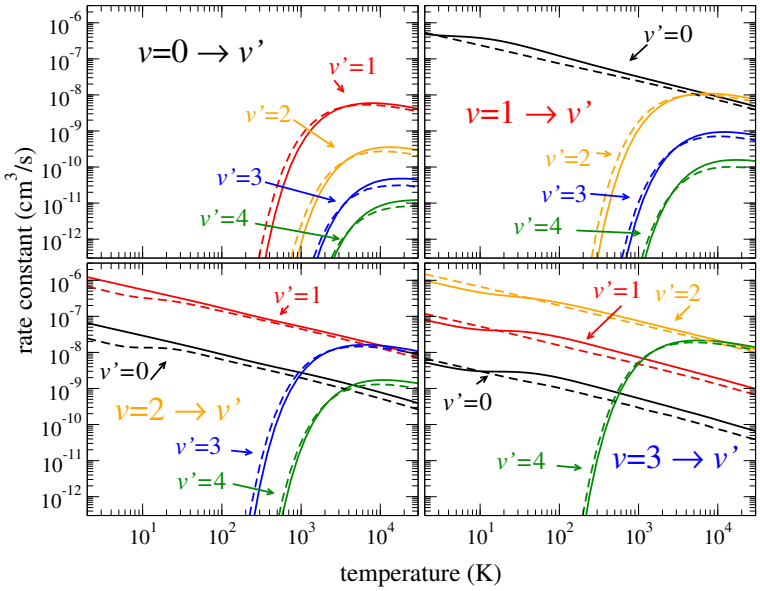

Figure 3. Same as Figure 2 for $^3HeH^+$ (solid lines) and $^3HeD^+$ (dashed lines).

The coefficients a_i ($i = 0, 1, 2, 3$) are fitted for each pair of transitions $v' \leftrightarrow v$ and given in Tables 3–6. The numerical values of the coefficients a_i in the Tables are such that they give the rate coefficients in units of $cm^3 \cdot s^{-1}$, with the temperature in fitting Equation (5) being in kelvin.

Table 3. Parameters a_0, a_1, a_2, and a_3 of the fitting polynomials $P^{fit}_{vv'}(x) = P^{fit}_{v'v}(x)$ of Equation (4) for $^4HeH^+$. The upper line in the header of the table specifies the pairs of initial and final vibrational levels for which the parameters are fitted. For convenience, we also specify (the second line of the header) the threshold energy $\Delta_{v'v}$ for the excitation process of the corresponding pair. For all excitation and de-excitation processes, the same parameters a_i are used in Equations (4) and (5).

v–v'	0–1	0–2	0–3	0–4	1–2	1–3	1–4	2–3	2–4	3–4
$\Delta_{v'v}$ (K)	4187	7935	11,238	14,091	3747	7050	9903	3303	6156	2853
a_0	1.09×10^{-6}	8.84×10^{-8}	1.67×10^{-8}	3.59×10^{-9}	1.76×10^{-6}	2.26×10^{-7}	4.09×10^{-8}	1.81×10^{-6}	3.21×10^{-7}	2.54×10^{-6}
a_1	-4.53×10^{-8}	-2.73×10^{-9}	3.98×10^{-9}	-1.08×10^{-10}	7.35×10^{-11}	5.34×10^{-8}	-1.39×10^{-9}	3.78×10^{-7}	-1.03×10^{-8}	-3.60×10^{-8}
a_2	8.70×10^{-9}	6.49×10^{-10}	-8.73×10^{-10}	4.61×10^{-11}	-5.88×10^{-9}	-1.14×10^{-8}	5.87×10^{-10}	-5.85×10^{-8}	4.15×10^{-9}	1.62×10^{-8}
a_3	-6.80×10^{-10}	-5.77×10^{-11}	4.17×10^{-11}	-3.88×10^{-12}	3.17×10^{-10}	5.42×10^{-10}	-5.13×10^{-11}	2.29×10^{-9}	-3.43×10^{-10}	-1.22×10^{-9}

Table 4. Same as Table 3 for $^4HeD^+$.

v–v'	0–1	0–2	0–3	0–4	1–2	1–3	1–4	2–3	2–4	3–4
$\Delta_{v'v}$ (K)	3323	6381	9175	11,701	3058	5851	8378	2793	5319	2526
a_0	7.12×10^{-7}	1.97×10^{-8}	7.91×10^{-9}	1.39×10^{-9}	6.90×10^{-7}	1.53×10^{-7}	1.28×10^{-8}	2.20×10^{-6}	1.41×10^{-7}	1.67×10^{-6}
a_1	-2.48×10^{-8}	7.78×10^{-9}	6.27×10^{-10}	1.35×10^{-10}	1.28×10^{-7}	-7.04×10^{-9}	2.14×10^{-9}	-1.10×10^{-7}	1.20×10^{-8}	-4.68×10^{-9}
a_2	7.50×10^{-9}	3.46×10^{-10}	-9.16×10^{-11}	1.35×10^{-11}	6.84×10^{-9}	1.29×10^{-9}	1.80×10^{-10}	9.19×10^{-9}	2.99×10^{-9}	3.31×10^{-8}
a_3	-5.54×10^{-10}	-9.01×10^{-11}	1.13×10^{-12}	-2.15×10^{-12}	-1.48×10^{-9}	-1.00×10^{-10}	-3.35×10^{-11}	-3.32×10^{-10}	-3.69×10^{-10}	-2.86×10^{-9}

Table 5. Same as Table 3 for $^3HeH^+$.

v–v'	0–1	0–2	0–3	0–4	1–2	1–3	1–4	2–3	2–4	3–4
$\Delta_{v'v}$ (K)	4308	8147	11,513	14,397	3838	7204	10,088	3365	6250	2884
a_0	5.53×10^{-7}	9.34×10^{-8}	5.63×10^{-9}	3.88×10^{-9}	1.74×10^{-6}	8.98×10^{-8}	4.37×10^{-8}	1.29×10^{-6}	3.35×10^{-7}	2.60×10^{-6}
a_1	4.11×10^{-7}	-1.81×10^{-9}	3.19×10^{-9}	-1.14×10^{-10}	2.06×10^{-9}	3.77×10^{-8}	-1.45×10^{-9}	1.31×10^{-7}	-1.03×10^{-8}	-3.54×10^{-8}
a_2	-7.41×10^{-8}	4.50×10^{-10}	-8.26×10^{-11}	5.06×10^{-11}	-2.36×10^{-9}	-5.72×10^{-10}	6.33×10^{-10}	2.70×10^{-8}	4.24×10^{-9}	1.66×10^{-8}
a_3	3.60×10^{-9}	-4.83×10^{-11}	-1.79×10^{-11}	-4.33×10^{-12}	5.86×10^{-14}	-2.41×10^{-10}	-5.56×10^{-11}	-3.23×10^{-9}	-3.52×10^{-10}	-1.25×10^{-9}

Table 6. Same as Table 3 for $^3HeD^+$.

v–v'	0–1	0–2	0–3	0–4	1–2	1–3	1–4	2–3	2–4	3–4
$\Delta_{v'v}$ (K)	3485	6677	9574	12,175	3191	6089	8689	2897	5498	2600
a_0	7.60×10^{-7}	3.03×10^{-8}	9.47×10^{-9}	2.01×10^{-9}	8.97×10^{-7}	1.67×10^{-7}	2.20×10^{-8}	2.10×10^{-6}	2.14×10^{-7}	2.12×10^{-6}
a_1	-1.71×10^{-8}	8.90×10^{-9}	8.22×10^{-11}	-6.00×10^{-11}	9.90×10^{-8}	-1.77×10^{-9}	-1.07×10^{-9}	1.33×10^{-8}	-1.10×10^{-8}	-8.41×10^{-8}
a_2	5.77×10^{-9}	-2.88×10^{-10}	3.09×10^{-11}	3.88×10^{-11}	4.12×10^{-9}	1.85×10^{-10}	6.28×10^{-10}	-8.84×10^{-9}	5.43×10^{-9}	3.13×10^{-8}
a_3	-4.75×10^{-10}	-4.38×10^{-11}	-6.48×10^{-12}	-3.16×10^{-12}	-1.06×10^{-9}	-4.64×10^{-11}	-5.28×10^{-11}	3.98×10^{-10}	-4.37×10^{-10}	-2.22×10^{-9}

4. Rate Coefficients and Cross Sections for Rotational (De-)Excitation

The inelastic cross section for the rotational excitation or de-excitation process $j'\mu'v' \leftarrow j\mu v$ of a linear molecule by electron impact is obtained from the scattering matrix of Equation (2)

$$\sigma_{j'\mu'v'\leftarrow j\mu v}(E_{el}) = \frac{1}{2j+1}\frac{\pi}{k_j^2}\sum_{J,l,l'}(2J+1)\left|e^{i(l\pi/2+\sigma_l)}S^{J,phys}_{j'\mu'l'v';j\mu lv}e^{-i(l'\pi/2+\sigma_{l'})}\right|^2, \quad (7)$$

where σ_l is the Coulomb phase shift. The derivation of the above formula is given in paper II.

In the ground electronic state of $^4HeH^+$, the projection μ of the electronic angular momentum on the molecular axis of the target is zero. Therefore, for scattering energies below the first excited electronic state $A^1\Sigma^+$ of $^4HeH^+$, $\mu = \mu' = 0$ in Equation (7). Figure 4 gives examples of the cross sections obtained with Equation (7) for the $j = 3 \rightarrow j' = 0, 1, 2, 4$ transitions of $^4HeH^+$ and $^3HeH^+$. The cross sections exhibit a strong resonant character for both molecular ions as well as for the two other isotopologues. These resonances are washed out when thermally-averaged rate coefficients are computed, leading to similar rate coefficients at high temperatures T, as shown by solid lines in Figures 5 and 6. Similar results are observed for $^4HeD^+$ and $^3HeD^+$, shown in the figures by dashed lines. However, the thermally averaged coefficients at low temperatures are sensitive to exact positions and widths of the lowest resonances because the integral over thermal velocities at low temperatures T is determined only by small collision energies, $E_{el} \lesssim k_B T$. As a result, the rate coefficients for the $j = 2 \rightarrow j = 0$ transitions, for example, in Figures 5 and 6, are slightly different for different isotopologues.

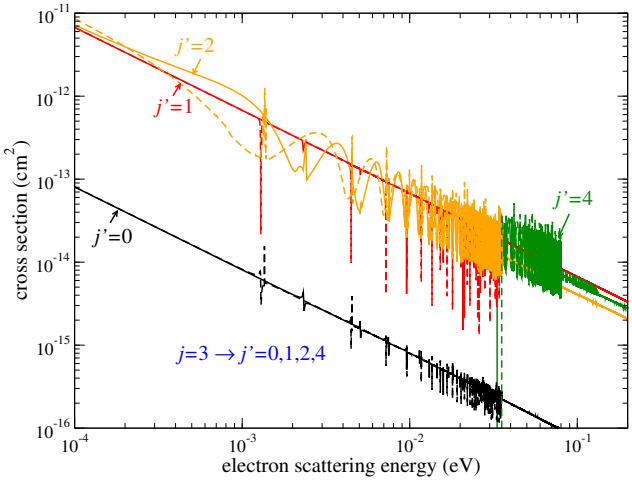

Figure 4. Cross sections of rotational (de-)excitation from the rotational level $j = 3$ to several other levels j' of $^4HeH^+$ (solid lines) and $^3HeH^+$ (dashed lines).

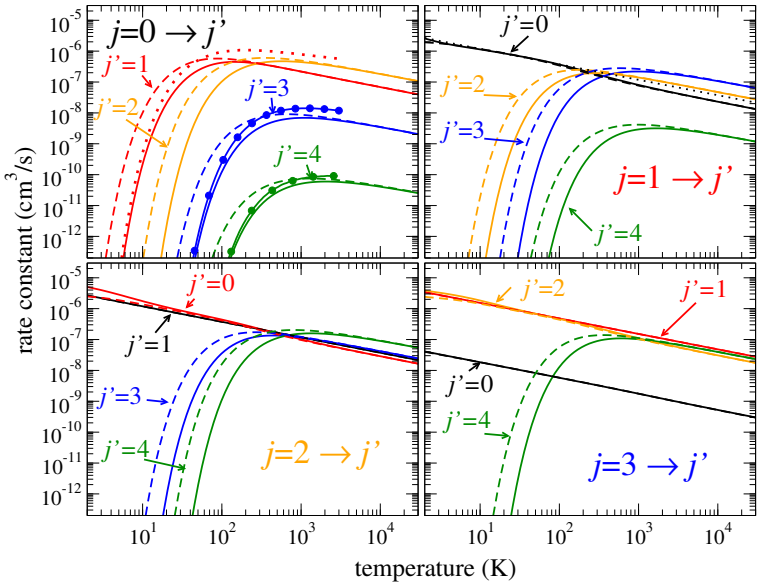

Figure 5. Thermally averaged rate coefficients for several rotational (de-)excitation transitions of ^{4}HeH$^+$ (solid lines) and ^{4}HeD$^+$ (dashed lines). Dotted lines in the upper-left panel are the calculations by Hamilton et al. [32], and lines with circles are those by Čurík and Greene [18] for ^{4}HeH$^+$.

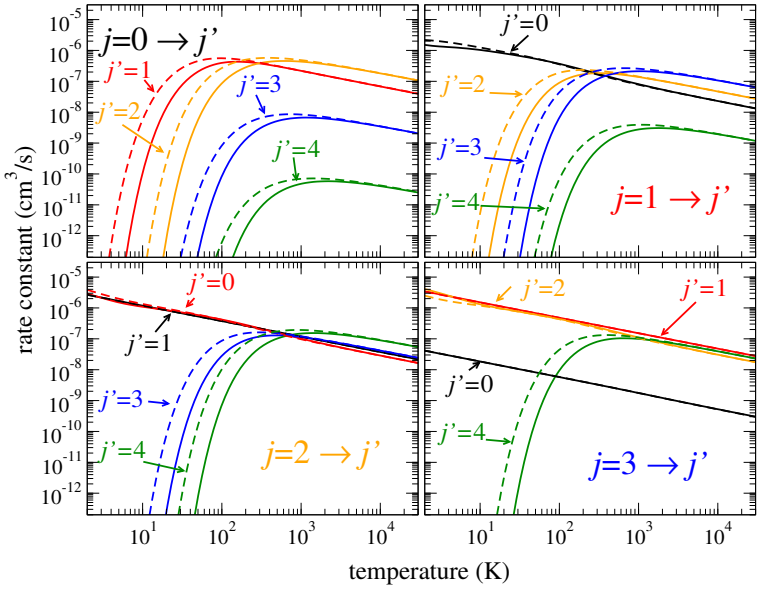

Figure 6. Same as Figure 5 for ^{3}HeH$^+$ (solid lines) and ^{3}HeD$^+$ (dashed lines). Rotational transition labels $j \to j'$ are shown in each panel.

In addition, the rotational rate coefficients behave approximately according to Equation (4), where $\Delta_{v'v}$ should be replaced with the rotational threshold energy, $\Delta_{j'j}$, and a quadratic polynomial is used in the fit. The probabilities for the direct $P^{fit}_{j'j}(x)$ ($j' \leftarrow j$) and the inverse $P^{fit}_{jj'}(x)$ ($j \leftarrow j'$) processes are related to each other by the relative degeneracy factor

$$P^{fit}_{j'j}(x) = \frac{2j'+1}{2j+1} P^{fit}_{jj'}(x)\,. \tag{8}$$

The coefficients a_i ($i = 0, 1, 2$) are fitted numerically for transitions $j' \leftrightarrow j$ and are given in Tables 7–10. Similarly to Tables in Section 3, the coefficients a_i give the rate coefficients in Equation (5) in units of cm^3/s.

Table 7. Parameters a_0, a_1, and a_2 of the polynomial $P_{jj'}^{fit}(x)$ of Equations (4) and (5) for several pairs of initial and final rotational states for de-excitation $j \leftarrow j'$ of $^4HeH^+$, with $j < j'$. The probabilities $P_{j'j}^{fit}(x)$ for the opposite (excitation) process, $j \rightarrow j'$, are obtained from $P_{jj'}^{fit}(x)$, multiplying them with the factor $(2j'+1)/(2j+1)$ (see Equation (8)). For convenience, we also specify, in the second line of the table, the threshold energy $\Delta_{j'j}$ in units of temperature (K) for the excitation process of the corresponding pair. For the de-excitation processes, $\Delta_{j'j} = 0$.

$j \leftarrow j'$	**0 ← 1**	**0 ← 2**	**0 ← 3**	**0 ← 4**	**1 ← 2**	**1 ← 3**	**1 ← 4**	**2 ← 3**	**2 ← 4**	**3 ← 4**
$\Delta_{j'j}$ **(K)**	**96**	**289**	**578**	**964**	**192**	**482**	**868**	**289**	**675**	**385**
a_0	3.90×10^{-6}	3.79×10^{-6}	5.80×10^{-8}	4.47×10^{-10}	7.36×10^{-6}	4.86×10^{-6}	7.60×10^{-8}	5.79×10^{-6}	5.36×10^{-6}	3.29×10^{-6}
a_1	-1.11×10^{-7}	-1.58×10^{-8}	3.35×10^{-10}	-2.17×10^{-12}	-8.57×10^{-7}	-8.43×10^{-9}	3.56×10^{-10}	-2.23×10^{-7}	8.55×10^{-10}	5.44×10^{-7}
a_2	-6.57×10^{-9}	1.03×10^{-9}	-9.66×10^{-11}	7.92×10^{-13}	3.99×10^{-8}	2.68×10^{-10}	-9.86×10^{-11}	-8.13×10^{-9}	-4.29×10^{-10}	-5.98×10^{-8}

Table 8. Same as Table 7 for $^4HeD^+$.

$j \leftarrow j'$	**0 ← 1**	**0 ← 2**	**0 ← 3**	**0 ← 4**	**1 ← 2**	**1 ← 3**	**1 ← 4**	**2 ← 3**	**2 ← 4**	**3 ← 4**
$\Delta_{j'j}$ **(K)**	**58**	**175**	**350**	**584**	**116**	**292**	**526**	**175**	**409**	**233**
a_0	2.79×10^{-6}	3.76×10^{-6}	5.55×10^{-8}	4.42×10^{-10}	3.43×10^{-6}	4.74×10^{-6}	7.73×10^{-8}	3.66×10^{-6}	5.39×10^{-6}	5.86×10^{-6}
a_1	2.67×10^{-7}	-5.03×10^{-9}	1.34×10^{-9}	-4.11×10^{-12}	2.84×10^{-7}	2.65×10^{-8}	4.68×10^{-10}	2.75×10^{-7}	-1.25×10^{-8}	-3.14×10^{-7}
a_2	-3.52×10^{-8}	2.30×10^{-10}	-1.82×10^{-10}	1.12×10^{-12}	-3.78×10^{-8}	-2.11×10^{-9}	-1.35×10^{-10}	-3.71×10^{-8}	6.95×10^{-10}	1.99×10^{-9}

Table 9. Same as Table 7 for $^3HeH^+$.

$j \leftarrow j'$	**0 ← 1**	**0 ← 2**	**0 ← 3**	**0 ← 4**	**1 ← 2**	**1 ← 3**	**1 ← 4**	**2 ← 3**	**2 ← 4**	**3 ← 4**
$\Delta_{j'j}$ **(K)**	**102**	**308**	**616**	**1026**	**205**	**513**	**924**	**308**	**718**	**410**
a_0	2.31×10^{-6}	3.77×10^{-6}	5.83×10^{-8}	4.47×10^{-10}	4.24×10^{-6}	4.86×10^{-6}	7.67×10^{-8}	5.87×10^{-6}	5.41×10^{-6}	6.84×10^{-6}
a_1	4.23×10^{-7}	-1.03×10^{-8}	2.04×10^{-10}	-1.62×10^{-12}	-9.42×10^{-8}	-1.53×10^{-8}	8.33×10^{-11}	-5.04×10^{-7}	-1.61×10^{-8}	-7.11×10^{-7}
a_2	-4.59×10^{-8}	6.82×10^{-10}	-8.59×10^{-11}	7.16×10^{-13}	-5.05×10^{-9}	9.74×10^{-10}	-7.62×10^{-11}	2.25×10^{-8}	8.80×10^{-10}	3.47×10^{-8}

Table 10. Same as Table 7 for $^3HeD^+$.

$j \leftarrow j'$	**0 ← 1**	**0 ← 2**	**0 ← 3**	**0 ← 4**	**1 ← 2**	**1 ← 3**	**1 ← 4**	**2 ← 3**	**2 ← 4**	**3 ← 4**
$\Delta_{j'j}$ **(K)**	**64**	**194**	**388**	**647**	**129**	**323**	**583**	**194**	**453**	**259**
a_0	2.98×10^{-6}	3.79×10^{-6}	5.86×10^{-8}	4.43×10^{-10}	5.98×10^{-6}	4.81×10^{-6}	7.67×10^{-8}	3.79×10^{-6}	5.37×10^{-6}	3.44×10^{-6}
a_1	2.62×10^{-7}	-1.13×10^{-8}	2.83×10^{-10}	-3.64×10^{-12}	-6.35×10^{-7}	-7.76×10^{-9}	5.76×10^{-10}	1.04×10^{-7}	-3.24×10^{-9}	4.46×10^{-7}
a_2	-3.71×10^{-8}	6.05×10^{-10}	-1.03×10^{-10}	1.05×10^{-12}	3.24×10^{-8}	8.42×10^{-10}	-1.38×10^{-10}	-1.95×10^{-8}	-3.95×10^{-11}	-5.17×10^{-8}

5. Conclusions

We presented cross sections and thermal rate coefficients for rotational and vibrational transitions in the stable isotopologues of the HeH^+ ion caused by electron impact. The differences observed in cross sections for the four isotopologues are due to different positions of vibrational and rotational levels of the target ion. The different positions of the levels produce Rydberg resonances in the collisional spectra that are situated at different energies. Different positions of individual resonances can significantly modify cross sections. This is especially important at low energies, as demonstrated in Figures 1 and 4. Very different cross sections at low collision energies lead to very different thermal rate coefficients at low temperatures.

Because the overall coupling between different vibrational and rotational channels is the same for all isotopologues, generally, widths of the resonances are comparable for the four isotopologues. This results in thermally averaged rate coefficients that are very similar in magnitude to each other for the four isotopologues. The only essential effect on the rate coefficients is due to a higher density of rovibrational levels and, as a result, a higher density of resonances in the collisional spectra for heavier isotopologues. This effect is evident in Figures 5 and 6 showing the coefficients for rotational excitation: For heavier isotopologues, the rotational excitation rate coefficients are, in general, higher. For vibrational transitions, the ratio of densities of vibrational resonances between different isotopologues is closer to unity compared to the rotational-level densities. Therefore, the isotope effect on the vibrational excitation coefficients is less important.

We extended our previous studies on $^4HeH^+$ to its isotopologues $^4HeD^+$, $^3HeH^+$, and $^3HeD^+$. The obtained results are important for hydrogen–helium plasma modeling and diagnostics and could contribute to the search of the $^4HeH^+$ isotopologues in astrophysical environments.

Author Contributions: All authors contributed equally to this work.

Funding: This research was funded by Grant No. PHY-1806915 of the National Science Foundation, the Thomas Jefferson Fund of the Office for Science and Technology of the Embassy of France in the United States and by the program "Accueil des chercheurs étrangers" of CentraleSupélec.

Acknowledgments: The authors are grateful to the referees for the constructive comments and improvement suggestions.

Conflicts of Interest: The authors declare no conflict of interest.

References and Note

1. Dabrowski, I.; Herzberg, G. The predicted infrared spectrum of HeH^+ and its possible astrophysical importance. *Trans. N. Y. Acad. Sci.* **1977**, *38*, 14. [CrossRef]
2. Black, J. Molecules in planetary nebulae. *Astrophys. J.* **1978**, *222*, 125. [CrossRef]
3. Flower, D.; Roueff, E. On the formation and destruction of HeH^+ in gaseous nebulae and the associated infra-red emission line spectrum. *Astron. Astrophys.* **1979**, *72*, 361.
4. Zygelman, B.; Dalgarno, A. The radiative association of He^+ and H. *Astrophys. J.* **1990**, *365*, 239. [CrossRef]
5. Kraemer, W.; Špirko, V.; Juřek, M. Formation of HeH^+ by radiative association of He^+ + H. An advanced ab initio study. *Chem. Phys. Lett.* **1995**, *236*, 177–183. [CrossRef]
6. Güsten, R.; Wiesemeyer, H.; Neufeld, D.; Menten, K.M.; Graf, U.U.; Jacobs, K.; Klein, B.; Ricken, O.; Risacher, C.; Stutzki, J. Astrophysical detection of the helium hydride ion HeH^+. *Nature* **2019**, *568*, 357. [CrossRef] [PubMed]
7. Heyminck, S.; Graf, U.; Güsten, R.; Stutzki, J.; Hübers, H.; Hartogh, P. GREAT: The SOFIA high-frequency heterodyne instrument. *Astron. Astrophys.* **2012**, *542*, L1. [CrossRef]
8. Zijlstra, A.A.; Van Hoof, P.; Perley, R. The evolution of NGC 7027 at radio frequencies: A new determination of the distance and core mass. *Astrophys. J.* **2008**, *681*, 1296. [CrossRef]
9. Liu, X.W.; Barlow, M.; Cox, P.; Péquignot, D.; Clegg, P.; Swinyard, B.; Griffin, M.; Baluteau, J.; Lim, T.; Skinner, C.; et al. The ISO LWS grating spectrum of NGC 7027. *Astron. Astrophys.* **1996**, *315*, L257–L260.

10. Liu, X.W.; Barlow, M.; Dalgarno, A.; Tennyson, J.; Lim, T.; Swinyard, B.; Cernicharo, J.; Cox, P.; Baluteau, J.P.; Pequignot, D.; et al. An ISO Long Wavelength Spectrometer detection of CH in NGC 7027 and an HeH^+ upper limit. *Mon. Not. R. Astron. Soc.* **1997**, *290*, L71–L75. [CrossRef]
11. Strömholm, C.; Semaniak, J.; Rosén, S.; Danared, H.; Datz, S.; van der Zande, W.; Larsson, M. *Phys. Rev. A* **1996**, *54*, 3086.
12. Tanabe, T.; Katayama, I.; Ono, S.; Chida, K.; Watanabe, T.; Arakaki, Y.; Haruyama, Y.; Saito, M.; Odagiri, T.; Hosono, K.; et al. Dissociative recombination of HeH^+ isotopes with an ultra-cold electron beam from a superconducting electron cooler in a storage ring. *J. Phys. B At. Mol. Opt. Phys.* **1998**, *31*, L297. [CrossRef]
13. Larson, Å.; Orel, A. Wave-packet study of the products formed in dissociative recombination of HeH^+. *Phys. Rev. A* **2005**, *72*, 032701. [CrossRef]
14. Takagi, H. Theoretical study of the dissociative recombination of HeH^+. *Phys. Rev. A* **2004**, *70*, 022709. [CrossRef]
15. Larson, Å.; Nkambule, S.; Ertan, E.; Söder, J.; Orel, A.E. Studies of HeH: DR, RIP, VE, DE, PI, MN, ... *EPJ Web Conf.* **2015**, *84*, 03001. [CrossRef]
16. Takagi, H.; Tashiro, M. Study on the dissociative recombination of HeH^+ by multi-channel quantum defect theory. *EPJ Web Conf.* **2015**, *84*, 02002. [CrossRef]
17. Rabadán, I.; Sarpal, B.K.; Tennyson, J. Calculated rotational and vibrational excitation rates for electron-HeH^+ collisions. *Mon. Not. R. Astron. Soc.* **1998**, *299*, 171. [CrossRef]
18. Čurík, R.; Greene, C.H. Inelastic low-energy collisions of electrons with HeH^+: Rovibrational excitation and dissociative recombination. *J. Chem. Phys.* **2017**, *147*, 054307. [CrossRef]
19. Ayouz, M.; Kokoouline, V. Cross Sections and Rate Coefficients for Vibrational Excitation of HeH^+ Molecule by Electron Impactukrm. *Atoms* **2016**, *4*, 30. [CrossRef]
20. Khamesian, M.; Ayouz, M.; Singh, J.; Kokoouline, V. Cross Sections and Rate Coefficients for Rotational Excitation of HeH^+ Molecule by Electron Impact. *Atoms* **2018**, *6*, 49. [CrossRef]
21. Tennyson, J. Electron–molecule collision calculations using the R-matrix method. *Phys. Rep.* **2010**, *491*, 29. [CrossRef]
22. Carr, J.; Galiatsatos, P.; Gorfinkiel, J.; Harvey, A.; Lysaght, M.; Madden, D.; Mašín, Z.; Plummer, M.; Tennyson, J.; Varambhia, H. UKRmol: A low-energy electron-and positron-molecule scattering suite. *Eur. Phys. J. D* **2012**, *66*, 58. [CrossRef]
23. Quantemol—A software tool maintained by Quantemol Ltd., which is based in University College London. The code brings a full accessibility to the UK molecular R-matrix code, which is used to model electron polyatomic molecule interactions.
24. Seaton, M.J. Quantum defect theory. *Rep. Prog. Phys.* **1983**, *46*, 167. [CrossRef]
25. Greene, C.H.; Jungen, C. Molecular applications ofquantum defect theory. *Adv. At. Mol. Phys.* **1985**, *21*, 51.
26. Aymar, M.; Greene, C.H.; Luc-Koenig, E. Multichannel Rydberg spectroscopy of complex atoms. *Rev. Mod. Phys.* **1996**, *68*, 1015. [CrossRef]
27. Kokoouline, V.; Dulieu, O.; Kosloff, R.; Masnou-Seeuws, F. Mapped Fourier methods for long-range molecules: Application to perturbations in the Rb_2 (0_u^+) photoassociation spectrum. *J. Chem. Phys.* **1999**, *110*, 9865. [CrossRef]
28. Coxon, J.; Hajigeorgiou, P. Experimental Born-Oppenheimer Potential for the $X^1\Sigma^+$ Ground State of HeH^+: Comparison with the Ab Initio Potential. *J. Mol. Spectrosc.* **1999**, *193*, 306–318. [CrossRef]
29. Stanke, M.; Kędziera, D.; Molski, M.; Bubin, S.; Barysz, M.; Adamowicz, L. Convergence of Experiment and Theory on the Pure Vibrational Spectrum of HeH^+. *Phys. Rev. Lett.* **2006**, *96*, 233002. [CrossRef]
30. Kokoouline, V.; Greene, C.H. Theory of dissociative recombination of D_{3h} triatomic ions applied to H_3^+. *Phys. Rev. Lett.* **2003**, *90*, 133201. [CrossRef]
31. Landau, L.; Lifshitz, E. *Quantum Mechanics: Non-Relativistic Theory*; Butterworth Heinemann: Burlington, MA, USA, 2003.
32. Hamilton, J.R.; Faure, A.; Tennyson, J. Electron-impact excitation of diatomic hydride cations–I. HeH^+, CH^+, ArH^+. *Mon. Not. R. Astron. Soc.* **2016**, *455*, 3281. [CrossRef]